Structure analysis of interstellar clouds - II. Applying the Delta-variance method to interstellar turbulence

Ossenkopf, V.; Krips, M.; Stutzki, J.

Published in:
Astronomy & astrophysics

DOI:
10.1051/0004-6361:20079107

Publication date:
2008

A&A 485, 719–727 (2008)
DOI: 10.1051/0004-6361:20079107

Astronomy & Astrophysics

Structure analysis of interstellar clouds

II. Applying the Δ-variance method to interstellar turbulence

V. Ossenkopf[1,2,3], M. Krips[1,4], and J. Stutzki[1]

[1] I. Physikalisches Institut der Universität zu Köln, Zülpicher Straße 77, 50937 Köln, Germany
e-mail: ossk@ph1.uni-koeln.de
[2] SRON Netherlands Institute for Space Research, PO Box 800, 9700 AV Groningen, The Netherlands
[3] Kapteyn Astronomical Institute, University of Groningen, PO box 800, 9700 AV Groningen, The Netherlands
[4] Harvard-Smithsonian Center for Astrophysics, SMA project, 60 Garden Street, MS 78 Cambridge, MA 02138, USA

Received 19 November 2007 / Accepted 22 February 2008

ABSTRACT

Context. The Δ-variance analysis is an efficient tool for measuring the structural scaling behaviour of interstellar turbulence in astronomical maps. It has been applied both to simulations of interstellar turbulence and to observed molecular cloud maps. In Paper I we proposed essential improvements to the Δ-variance analysis and tested them on artificial structures with known characteristics.
Aims. In this paper we apply the improved Δ-variance analysis to simulations of interstellar turbulence and observations of molecular clouds. We tested the new capabilities in practical use and studied properties of interstellar turbulence that could not have been addressed before.
Methods. We selected three example data sets that profit in particular from the improved Δ-variance method: i) a hydrodynamic turbulence simulation with prominent density and velocity structures; ii) an observed intensity map of ρ Oph with irregular boundaries and variable uncertainties of the different data points; and iii) a map of the turbulent velocity structure in the Polaris Flare affected by the intensity dependence on the centroid velocity determination.
Results. The tests confirm the extended capabilities of the improved Δ-variance analysis. Prominent spatial scales were accurately identified and artifacts from a variable reliability of the data were removed. The analysis of the hydrodynamic simulations showed that the injection of a turbulent velocity structure creates the most prominent density structures are produced on a scale somewhat below the injection scale. The new analysis of a ρ Oph continuum map reveals an intermediate stage in the molecular cloud evolution showing both signatures of the typical molecular cloud scaling behaviour and the formation of condensed cores. When analysing the velocity structure of the Polaris Flare we show that a universal power law connects scales from 0.03 pc to 3 pc. However, a plateau in the Δ-variance spectrum around 5 pc indicates that the visible large-scale velocity gradient is not converted directly into a turbulent cascade here. It is obvious that, for any turbulent structure, effects of low-number statistics become important on the driving scale.

Key words. methods: data analysis – methods: statistical – ISM: clouds – ISM: structure

1. Introduction

Observations of interstellar clouds show a complex, filamentary structure which can be attributed to turbulence in the interstellar medium (Franco & Carramiñana 1999; Ossenkopf et al. 2000; Mac Low & Klessen 2004). To understand the processes governing the structure and evolution of the clouds, turbulence models have to be constructed and compared to observational data. Their parameters and implementational details need to be adjusted to fit the observed behaviour. Due to the random nature of turbulence, simulations will never provide an exact reproduction of the observed data sets but will only reproduce general statistical properties like scaling relations.

The most common scaling relation to characterise turbulent structures is the power spectrum of fluctuations, both in density and in velocity. Here, we encourage using another quantity, the Δ-variance spectrum, introduced by Stutzki et al. (1998), a wavelet-based method to measure the relative amount of structural variation as a function of the size scale. Due to the mutual relations between the Δ-variance spectrum and the radially averaged power-spectrum, the Δ-variance analysis can be considered as a very robust method of evaluating the power spectrum of a structure. The advantages of the Δ-variance method result from the smooth wavelet filter shape, which provides a robust way for an angular average independent of gridding effects, and from the insensitivity to edge effects as discussed by Bensch et al. (2001).

In parallel to the structure scaling analysis, clump decomposition algorithms like GAUSSCLUMP (Stutzki & Güsten 1990) found that the clump mass spectrum $\mathrm{d}N/\mathrm{d}M \propto M^{-\gamma}$ of sufficiently large molecular cloud data sets also tend to follow power laws over many orders of magnitude with the spectral index γ in a relatively narrow range between 1.7 to 1.9 (Kramer et al. 1998; Heithausen et al. 1998). Stutzki et al. (1998) demonstrated that a clump ensemble with such a mass spectrum and with a power-law mass-size scaling relation results in a cloud image with the Δ-variance scaling index determined by the number-mass and the mass-size spectral indices. However, it was questioned by e.g. Vázquez-Semadeni et al. (1997); Ballesteros-Paredes & Mac Low (2002) whether the observed mass-size relation reflects true properties of the underlying structure. It may rather represent an observational artifact. From these results it is obvious that there is a strong interest in studying the spatial scaling behaviour of observed maps of the interstellar medium via the Δ-variance analysis.

In Paper I we have proposed several essential improvements to the original Δ-variance method. We have investigated the use of different wavelets and calibrated their spatial resolution. Unfortunately, it turns out that it is not possible to define a

single optimum wavelet for all purposes because different wavelets exhibit a different power in the detection of the characteristic structures. A good compromise is given by the Mexican-hat filter with a diameter ratio of 1.5. When the main focus lies on the measurement of the spectral index, the French-hat filter with a diameter ratio of about 2.3 is also suitable. We also introduced a significance function to weight the different data points. This allows us to analyse observed data where the signal-to-noise ratio is not uniform across the mapped area, but spatially varying. This should permit to distinguish the influence of variable noise from actual small-scale structure in the maps. The need for such a treatment became very obvious when Ossenkopf & Mac Low (2002) used the Δ-variance analysis to characterise the velocity structure detected in molecular line observations of the Polaris Flare taken by Falgarone et al. (1998), Bensch et al. (2001), and Heithausen & Thaddeus (1990). Comparing the Δ-variance analysis with the size-linewidth relation, we found that the Δ-variance of the centroid velocity maps produced wrong results on scales where the maps do not show any noticeable emission. With the introduction of the significance function, the new Δ-variance analysis should be able to also reliably analyse such data sets. Moreover, the use a weighting function also allows us to use computational methods like the fast Fourier transform to obtain the Δ-variance spectrum even for maps with irregular boundaries or maps which are only sparsely filled by significant values.

In Paper I we tested the properties of the improved Δ-variance analysis using simple artificial data sets. In this paper we will apply it to more realistic data sets, either simulations of interstellar turbulence or to actual observational data. In Sect. 2 we recapitulate the formalism of the new Δ-variance analysis and summarise the results that we obtained from the application to the test data sets. In Sect. 3 we apply the analysis to a hydrodynamic simulation, to the ρ-Oph dust continuum map by Motte et al. (1998) and to the centroid velocity map for the Polaris Flare. We discuss the conclusions on their structure in Sect. 4.

2. The improved Δ-variance method

In this section we summarise the main properties of the improved Δ-variance analysis proposed in Paper I, focusing on the new points, not covered in the original Δ-variance definition by Stutzki et al. (1998).

The Δ-variance measures the amount of structure on a given scale l in a map $f(\boldsymbol{r})$ by filtering the map with a spherically symmetric wavelet of size l and computing the variance of the thus filtered map:

$$\sigma^2_\Delta(l) = \left\langle \left(f(\boldsymbol{r}) * \bigodot_l(\boldsymbol{r}) \right)^2 \right\rangle_{\boldsymbol{r}} \tag{1}$$

where, the average is taken over the area of the map, the symbol $*$ stands for a convolution, and $\bigodot_l$ describes the filter function composed of positive inner "core" and a negative annulus, both normalised to integral values of unity

$$\bigodot_l(\boldsymbol{r}) = \bigodot_{l,\mathrm{core}}(\boldsymbol{r}) - \bigodot_{l,\mathrm{ann}}(\boldsymbol{r}). \tag{2}$$

We have studied the "French-hat" filter with constant values in both parts:

$$\bigodot_{l,\mathrm{core}}(\boldsymbol{r}) = \frac{4}{\pi l^2} \begin{cases} 1 & : |\boldsymbol{r}| \le l/2 \\ 0 & : |\boldsymbol{r}| > l/2 \end{cases}$$

$$\bigodot_{l,\mathrm{ann}}(\boldsymbol{r}) = \frac{4}{\pi l^2} \begin{cases} 1/(v^2-1) & : l/2 < |\boldsymbol{r}| \le v \times l/2 \\ 0 & : |\boldsymbol{r}| \le l/2, |\boldsymbol{r}| > v \times l/2 \end{cases} \tag{3}$$

and a "Mexican hat" consisting of two Gaussian functions:

$$\bigodot_{l,\mathrm{core}}(\boldsymbol{r}) = \frac{4}{\pi l^2} \exp\left(\frac{\boldsymbol{r}^2}{(l/2)^2} \right) \tag{4}$$

$$\bigodot_{l,\mathrm{ann}}(\boldsymbol{r}) = \frac{4}{\pi l^2 (v^2-1)} \left[\exp\left(\frac{\boldsymbol{r}^2}{(vl/2)^2} \right) - \exp\left(\frac{\boldsymbol{r}^2}{(l/2)^2} \right) \right]$$

where l is the core diameter and v is the diameter ratio between the annulus and the core of the filter. Plotting the Δ-variance as a function of the filter size l then provides a spectrum showing the relative amount of structure in a given map as a function of the structure size.

The effective filter size, given by the average distance of points in the core and the annulus, deviates from the core diameter l as

$$\frac{l_{\mathrm{eff}}}{l} = \begin{cases} 0.29v + 0.26 & \text{for the French hat} \\ 0.41v + 0.46 & \text{for the Mexican hat.} \end{cases} \tag{5}$$

Thus structures with a particular size should show up as prominent peaks in the Δ-variance spectrum on a scale l_{eff} corresponding to that size. Test with artificial data sets in Paper I have shown, however, that the peak positions always falls 10–20% below the maximum structure size. Taking this systematic offset into account we can nevertheless reliably calibrate the spatial resolution of the Δ-variance analysis.

A major improvement of the new Δ-variance algorithm was the introduction of a weighting function to the data $w_{\mathrm{data}}(\boldsymbol{r})$. This simultaneously solved the problems of the edge treatment of finite maps and the analysis of data with a variable uncertainty across the map. The weight function varies between 0 and 1, representing the reliability of the individual data points, and it extends beyond the original map size, padding it with zeros at the boundaries. Instead of the original map $f(\boldsymbol{r})$, an extended map, $f_{\mathrm{padded}}(\boldsymbol{r}) = f(\boldsymbol{r}) \times w_{\mathrm{data}}(\boldsymbol{r})$ inside the original data area, $f_{\mathrm{padded}}(\boldsymbol{r}) = 0$ outside, is analysed. This padded map can be periodically continued without wrap-around effects, so that the filter convolution can be efficiently computed in Fourier space involving a fast Fourier transform and a map multiplication.

To avoid that data points within the padded area or with a low weighting are counted like normal zero-value data, but disregarded in the computation of the variance, the filter has to be renormalised at each position in the map in such a way that the integral weights of core and annulus remain unity when excluding the padded points and when taking the weighting of the normal data points into account. Instead of one convolution (Eq. (1)), one has to compute four convolutions

$$\begin{aligned} G_{l,\mathrm{core}}(\boldsymbol{r}) &= f_{\mathrm{padded}}(\boldsymbol{r}) * \bigodot_{l,\mathrm{core}}(\boldsymbol{r}') \\ G_{l,\mathrm{ann}}(\boldsymbol{r}) &= f_{\mathrm{padded}}(\boldsymbol{r}) * \bigodot_{l,\mathrm{ann}}(\boldsymbol{r}') \\ W_{l,\mathrm{core}}(\boldsymbol{r}) &= w(\boldsymbol{r}) * \bigodot_{l,\mathrm{core}}(\boldsymbol{r}') \\ W_{l,\mathrm{ann}}(\boldsymbol{r}) &= w(\boldsymbol{r}) * \bigodot_{l,\mathrm{ann}}(\boldsymbol{r}') \end{aligned} \tag{6}$$

and combine the results while re-normalising with the effective filter weight for the valid data

$$F_1(\boldsymbol{r}) = \frac{G_{l,\mathrm{core}}(\boldsymbol{r})}{W_{l,\mathrm{core}}(\boldsymbol{r})} - \frac{G_{l,\mathrm{ann}}(\boldsymbol{r})}{W_{l,\mathrm{ann}}(\boldsymbol{r})}. \tag{7}$$

From the actual filter weight computed for each point in the map we can derive a significance function as the product of both normalisation factors

$$W_{l,\mathrm{tot}}(\boldsymbol{r}) = W_{l,\mathrm{core}}(\boldsymbol{r}) W_{l,\mathrm{ann}}(\boldsymbol{r}). \quad (8)$$

This provides the actual significance of the data points in the convolved map which is used when computing the Δ-variance of the whole map

$$\sigma^2_\Delta(l) = \frac{\sum_{\mathrm{map}} (F_1(\boldsymbol{r}) - \langle F_1 \rangle)^2 W_{l,\mathrm{tot}}(\boldsymbol{r})}{\sum_{\mathrm{map}} W_{l,\mathrm{tot}}(\boldsymbol{r})} \,. \quad (9)$$

With this generalised concept, the Δ-variance analysis can be applied to arbitrary data sets. They must be projected onto some regular grid but they do not need to contain regular boundaries as the corresponding "empty" grid points can be marked with a zero significance. Varying noise or other changes in the data reliability can be expressed in the significance function $w_{\mathrm{data}}(\boldsymbol{r})$. This applies e.g. to maps where not all points are observed with the same integration time so that they show a different noise level. In Paper I we used a weighting function given by the inverse noise rms and in Sect. 3.2 we will study the impact of the selection of the weighting function for observed data.

The only remaining requirement for the applicability of the Δ-variance analysis is a sufficiently large spatial dynamic range in the data. Bensch et al. (2001) had shown that a map has to contain at least 30 pixels in each direction to obtain reasonable error bars of the Δ-variance spectrum. Numerical tests with noisy data in Paper I showed that this critical size needs to be extended by a factor of about one over the average data significance in the case of data with a variable reliability.

3. Applications

3.1. Hydrodynamic simulations

In the papers by Mac Low & Ossenkopf (2000), Ossenkopf & Mac Low (2002), and Ossenkopf et al. (2001) we have demonstrated the general applicability of the Δ-variance analysis to extract characteristic structure sizes and scaling laws from (magneto-)hydrodynamic simulations performed with a variety of codes. Here, we need to test whether the Δ-variance with adapted filter functions improves the sensitivity of this method. The weighting function is irrelevant in this case because the data do not suffer from noise or another cause of variable reliability across the data set.

We have applied the analysis to a variety of simulations presented in Ossenkopf et al. (2001), but we present the results here only for a single model, the first inertial stage of the small-scale driven hydrodynamic turbulence computed by smooth-particle hydrodynamics (SPH), S02 at $t = 0$. In this simulation the velocity field is driven by a Gaussian field of random fluctuations within a finite wavenumber range, $k = 7 \ldots 8$. This means, that the driving process introduces characteristic variations into the velocity structure with the same scale length as used in the artificial sine wave field used in Paper I, but with wavenumbers between 7 and 8. Thus the Δ-variance spectrum should measure a peak variation for scales of $1/(\sqrt{2}k)$, i.e. between 0.088 and 0.101 of the size of the whole data cube. Selecting a model which is driven on small scales guarantees that we can identify a clear peak for these structures leaving enough dynamic range on smaller and larger scales. We select the initial stage of fully evolved turbulence in the simulation to make sure that the turbulent driving is the only process creating structures in the data set, avoiding effects of self-gravity. In this way we have a data set which is best suited to test the structure recognition by the Δ-variance analysis, as it should directly detect the scales of the driving process in the velocity structure and determine the scaling of the turbulent cascade on lower scales. Results for the other simulations did not provide any fundamentally different results, but are less clear to interpret because either the driving scale is closer to the edge of the dynamic range or the contained structure is less well known.

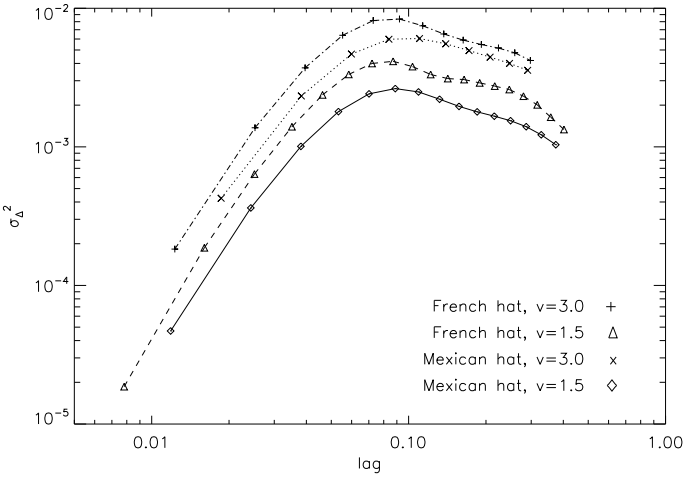

Fig. 1. Δ-variance spectra of the z-projection of the z-component of the velocity field in the hydrodynamic simulation S02 at $t = 0$. Four different filter shapes are tested against each other.

Figure 1 shows the Δ-variance spectra of the z-projection of the z component of the velocity field of the turbulence simulation computed with four different filter functions. We find a clear shift between the peak positions measured by the different filters. The Mexican-hat filter gives systematically larger lags for the peak than the French hat and the lag of the peak grows with growing annulus-to-core diameter ratio, υ. The minimum peak lag, given by the French hat with $\upsilon = 1.5$, falls at 0.084, the maximum lag, given by the Mexican hat with $\upsilon = 3$, at 0.11.

This behaviour is consistent with the results obtained for the simple sine wave field in Paper I. It can be understood as a result of the variable width and the shape of the filters in Fourier space. The broadening of the filter function reduces the contrast which leads in a spectrum with a steep slope on small scales and a shallow slope on large scales to an effective shift of the peak position. The steep decay of the French-hat filter function for large lags leads to a somewhat lower peak position, but is always accompanied by side lobes of the Bessel function visible as artificial secondary peaks at large lags. For the turbulence simulations these secondary peaks are not as pronounced as for the sine wave field, but they are also visible in Fig. 1. For the diameter ratios υ of about 1.5 for the Mexican hat and 2.3 for the French hat, deduced as optimum values in Paper I, the peak position falls at about 0.088 in both cases, a value slightly lower than the expected average structure size.

The different width of the peak has a direct impact on the slope of the turbulent structures measured at small lags. With the broad peaks produced by the Mexican-hat filter, the slope is affected down to relatively small scales. As the filter diameter ratio υ constrains the minimum scale which can be resolved, a clear power law becomes only visible for the French-hat filter with $\upsilon = 1.5$. Small diameter ratios are always favourable with respect to the dynamic range which can be covered in the Δ-variance analysis because of the minimum filter size and the

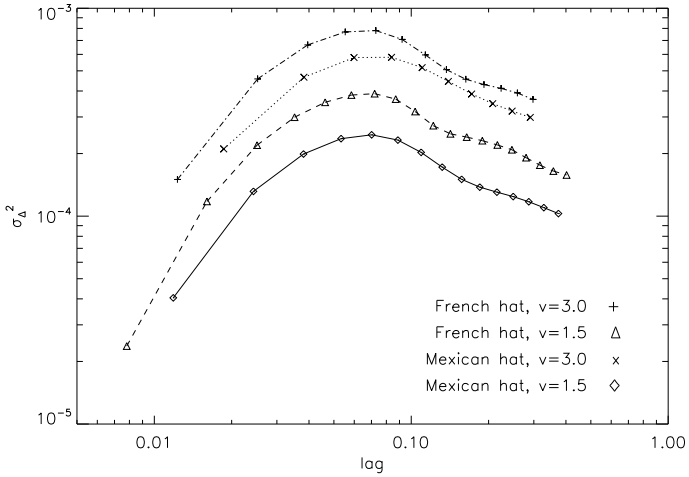

Fig. 2. Δ-variance spectra of the density structure created by the velocity field from Fig. 1, measured with four different filter functions.

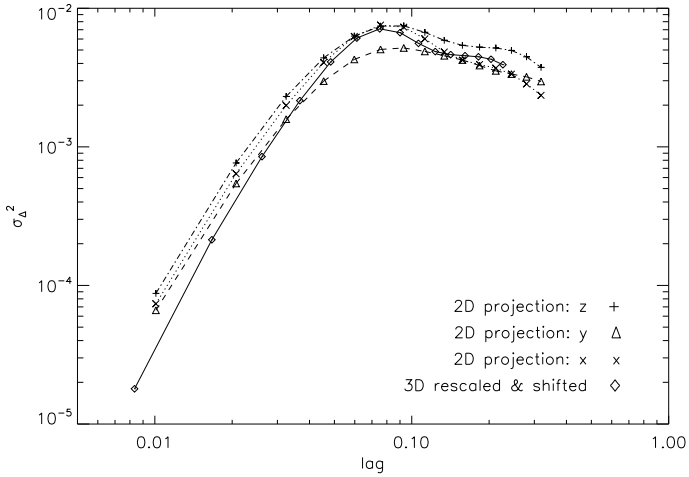

Fig. 3. Δ-variance spectra of the different rectangular projection maps and of the full three-dimensional data cube of the z-component of the velocity field in simulation S02 at $t = 0$. The analysis used the French-hat filter with a annulus-to-core diameter ratio $v = 2.3$.

constraint that the overall filter must always remain small compared to the analysed map. For the French hat with $v = 3.0$ and the Mexican hat with $v = 1.5$ the remaining dynamic range is just marginally sufficient to reliably determine the spectral index. We find slopes between 2.8 and 3.1 corresponding to power spectral indices $\zeta = 4.8 \ldots 5.1$. This is much higher than the Kolmogorov index of $\zeta = 3.67$ indicating that the scaling on small scales is not determined by a self-similar turbulent cascade, but by the numerical viscosity in these simulations damping small scale structures. For simulations driven on large scales resulting in a larger dynamic range below the peak, we find a limited inertial range with a slope of about two, corresponding to $\zeta \approx 4$ which is consistent with a cascade of Burger's turbulence (see Ossenkopf & Mac Low 2002; Ossenkopf et al. 2001).

In a second step we investigate how the turbulent velocity scaling translates into the creation of turbulent density enhancements. Figure 2 shows the Δ-variance spectra of the density structure seen in the same step of the simulation using the same filters as applied to the velocity structure. We find the same systematic deviations between the results seen by different filters but a generic shift of the peak position to shorter lags by a factor 0.75–0.8 with respect to the peaks of the velocity structure. The slope of the turbulent density structure on small scales is shallower by 1.0 ± 0.05. For the mutual comparison between density and velocity structure, the selection of the filter is thus irrelevant as long as the same filter is applied in both cases.

We see that injesting energy on a particular scale does not create density enhancements on that scale, but rather on a scale smaller by a factor 0.75–0.8. This shift has not been noticed before by Mac Low & Ossenkopf (2000) as only the systematic tests of the filter functions provided enough sensitivity with respect to a reliable scale detection. It seems that the turbulent cascade builds up density fluctuations on all scales below the driving scale, but that those density enhancements act themselves as points of an efficient energy conversion between the scales creating new density structures so that dominant density scale falls somewhat below the initial scale.

Finally we need to address the significance of the measured structure size and the scaling indices with respect to the random fluctuations always present in turbulence simulations and with respect to the relation between the three-dimensional (3-D) structure and the two-dimensional (2-D) projections which we can measure in astronomical observations. For turbulent density structures this comparison has been done by Mac Low & Ossenkopf (2000) using the "traditional" Δ-variance filter with the diameter ratio $v = 3.0$. We will repeat it here for the velocity structure as the direct carrier of turbulent energy using one of more sensitive filter functions.

Figure 3 shows the Δ-variance spectra of the z-component of the hydrodynamic simulation introduced above, computed with a French-hat filter with $v = 2.3$. The three broken lines show the Δ-variance spectra computed for the three different orthogonal projections of the velocity data cube. The solid curve shows the spectrum computed for the 3-D structure but rescale as if computed in 2-D by a factor proportional to the lag, to compensate for the different exponents of the Δ-variance spectra depending on the dimensionality of the considered space, and shifted by a factor $\pi/4$, to account for the average reduction of a random structure size when projected from 3-D onto a plane. The solid line, thus represents our best knowledge on the velocity structure actually present in the simulations, while the broken lines represent possible observer's views onto that structure.

We find a considerable variation between the Δ-variance spectra seen in the different directions, giving a feeling for the statistical uncertainty when measuring the scaling in turbulent simulations[1]. Nevertheless, both the peak position and the exponent at small lags agree between all three curves. Compared to the full 3-D structure, there is, however, a systematic shift of the peak to somewhat larger lags and a slight reduction of the slope at small lags. For the 3-D structure the peak is seen at a lag of about 0.075, which is about 20% smaller than the expected scale for the maximum variation, while the peak for the projections falls between 0.081 and 0.092, i.e. only 10% below the expected scale. In the 2-D projections, the peak is always broader and the slope at small lags is always somewhat shallower, similar to the impact of broader filter functions. It is important to notice, that the corresponding plots for the turbulent density structure, showing a shallower scaling at small lags, exhibit a very good match between the Δ-variance spectra computed in 2-D and in 3-D, i.e. neither a shift of the peak nor different slopes at small lags.

This seems to indicate that the turbulent velocity cascade does not behave fully isotropic. A similar effect would be expected for grid-based hydrodynamic simulations where the

[1] The computational uncertainty given by the finite size of any data set was discussed in detail by Bensch et al. (2001).

dissipation is strong between neighbouring cells in the x-, y-, and z-directions. However, the simulations studied here used an SPH code which should not show any intrinsic anisotropy. The cause for the anisotropy of the turbulent velocity scaling is thus so far unknown.

3.2. Maps with variable noise

Maps with variable noise are obtained e.g. in observations with detector arrays showing a pixel-to-pixel variation in the sensitivity. They are produced in single-pixel observations when a drift in the receiver sensitivity or the atmospheric conditions changes the noise in the data during the measurement and they result from mosaicing observations with variable integration times for different regions of the field. All these cases can be analysed in terms of the improved Δ-variance as long as the spatial distribution of the noise across the map is well known so that a corresponding significance map can be defined which is used to weight the different points in the Δ-variance analysis. Then the Δ-variance spectrum is able to distinguish between small-scale noise contributions in regions with a high noise level and real small-scale structures in regions with a low noise level.

As a challenging example of a data set where a variable noise is produced by the observation of different points of the map with varying integration time we use the 1.3 mm continuum map of ρ Oph obtained by Motte et al. (1998). It is the result of a mosaicing observation where an efficient use of the array receiver is given by several observations of the source with different orientations of the array. The combination of these observations then results in a poorer coverage of the outer regions of the source compared to the central regions in terms of the total integration time spent on each point. If the source is covered in total with $N_{\rm tot}$ observations, we can characterise the integration time at each point by the number of coverages including this point $1 \le N \le N_{\rm max}$, where $N_{\rm max} \le N_{\rm tot}$. As the noise at each point is inversely proportional to the square root of the integration time, we can use the value of $\sqrt{N}$ as a measure for the data reliability across the map.

In addition to the variable noise the map has highly irregular boundaries. Figure 4 shows the intensity map. In contrast to the original publication we show the intensity with equidistant contours on a linear scale because the linear-scale presentation gives a better feeling for the structure that is measurable by means of a statistical method like the Δ-variance analysis. To emphasise the irregular noise behaviour we plot one contour at 20 mJy/15″-beam, which is below the noise level in the outer parts of the map and above the noise level in the inner parts. Consequently, this contour shows partly real structure and partly artificial structure from the noise. Figure 5 contains the corresponding map of significance values defined as the square root of the number of integrations at each point, $\sqrt{N}$, thus measuring the inverse noise rms.

To demonstrate the influence of the significance weighting we show in Fig. 6 the Δ-variance spectra computed for the ρ Oph map using three different weighting functions. The lower spectrum is generated when the weights are ignored, i.e. simply set to unity at all valid data points. The upper graph is produced when the full weighting function from Fig. 5 is used. The intermediate curve follows when we introduce and upper limit to the weighting function motivated by the idea that above a certain significance limit a further reduction of the noise level does not improve the structure characterisation any more. All computations use the filter truncation outside of the area where data

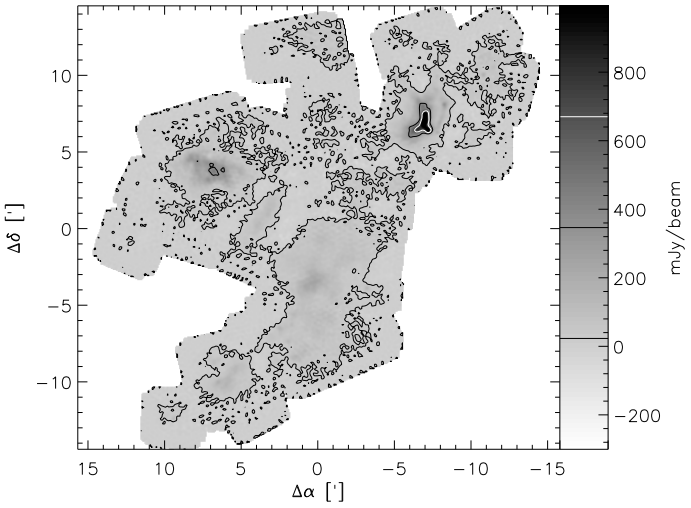

Fig. 4. 1.3 mm continuum map of ρ Oph taken by Motte et al. (1998). The intensity is normalised to a 15″ beam. In contrast to Motte et al. we plot the intensity on a linear scale because the structure analysis by means of the Δ-variance only measures this linear behaviour. For a better contrast of the picture the intensity scale is truncated here at 1000 mJy/beam whereas the map contains a few points with intensities up to 1700 mJy/beam in the brightest core.

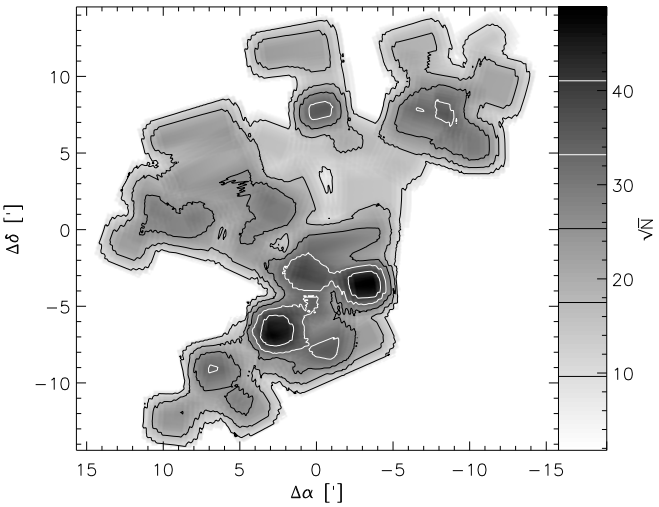

Fig. 5. Map of weights for the intensity map from Fig. 4 given by the square root of the number of integrations at each point.

have been taken. The irregular boundaries make it impossible to construct a useful periodic continuation here.

The Δ-variance spectrum computed without weights seems to indicate a wide range of scales with a power-law behaviour from about 0.2′ to 2′ whereas the Δ-variance spectrum computed with the full weights shows a steepening starting at 0.5–0.7′. Bensch et al. (2001) have shown, however, that such a behaviour is exactly to be expected from the finite beam of the observations. The data are given at a resolution of 15″ and the corresponding beam smearing is known to steepen the Δ-variance spectrum up to scales of about one arcminute. This steepening can be modelled theoretically using the analytic expressions for the beam convolution from Bensch et al. In fact, the Δ-variance spectrum computed from the ρ Oph map with full weights can be fitted by a single power-law structure with $\alpha = 0.68$ from $\lesssim$0.2′ up to about 2′ and a convolution function of a 15″ HPBW beam (see Fig. 7). The fitted exponent of 0.68 falls into the range measured in molecular line observations of molecular clouds

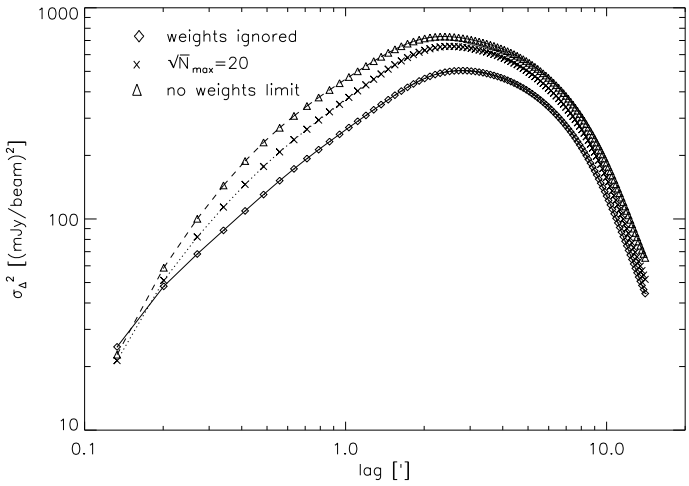

Fig. 6. Δ-variance spectra of the 1.3 mm ρ Oph map computed using three different weighting functions. Either all observational weights are ignored, they are completely taken into account, or weights above $\sqrt{N} = 20$ are set to this maximum level.

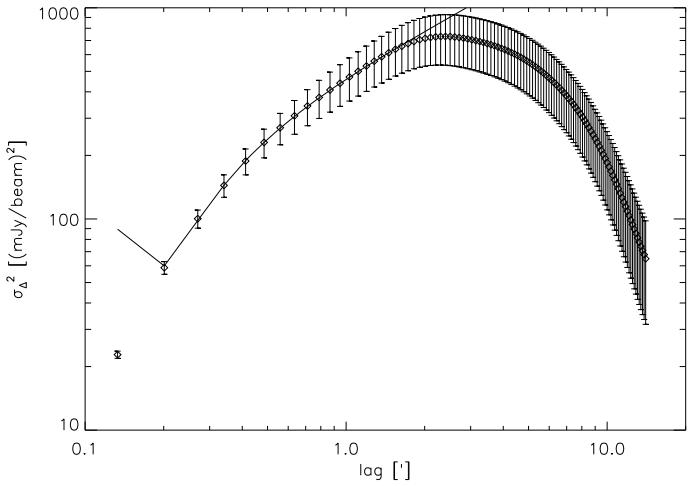

Fig. 7. Δ-variance spectrum for the ρ Oph continuum map with the full weighting function plotted with error bars indicating the statistical uncertainty of the measurement. The connecting line represents the power-law fit to the spectrum including the beam convolution effect. The point at the smallest lag cannot be fitted by the first order approximation of the beam shape (see Bensch et al. 2001).

covering exponents between 0.5 and 1.3 (Bensch et al. 2001; Elmegreen & Scalo 2004; Falgarone et al. 2004). In contrast, the two lower curves cannot be fitted in the same way. These spectra would lead to the conclusion of a surplus of small-scale structure relative to a power-law scaling relation. Such a relative surplus of structure on small scales is hard to explain as it would require additional driving processes on these scales overcompensating the known dissipation of turbulence by ambipolar diffusion and molecular viscosity (Klessen et al. 2000). Gravitational collapse is not able to create these structures; it always affects the whole Δ-variance spectrum, not only the small-scale tail (Ossenkopf et al. 2001). A surplus of small-scale structure is also in contrast to the analysis of Motte et al. (1998) who found a relative lack of small structures in terms of a flatter clump mass spectrum for small clumps.

Thus we conclude from the scaling behaviour that the full weighting of intensity maps by their inverse noise rms results in the most reliable Δ-variance spectra. With this weighting the Δ-variance analysis is able to distinguish insignificant small-scale structure, dominating the lowest contour in Fig. 4, from significant structures which are intuitively better presented by the contours chosen in the original plot by Motte et al.. The increase of the absolute value of the Δ-variance at large lags when using the weighting function is explained by the relative increase of the contribution of the bright cores in the map when virtually reducing the map size by weighting the outer parts by lower significance values.

To get a feeling for the reliability of the different points in the Δ-variance spectrum we plot in Fig. 7 the Δ-variance spectrum including the error bars. The error bars arise from the statistical uncertainty of the measurement of the average variance in a filtered map (Bensch et al. 2001). Due to the lower number of statistically independent points in maps convolved with a larger filter, the Δ-variance is most uncertain at the largest lags. In spite of the large error bars, the general scaling behaviour can be accurately traced. The solid line shows the fit to the data using a power-law description of the structure scaling and the convolution by a 15″ beam.

In the Δ-variance spectrum one can clearly see that the dominating structure has a scale of about 2.2′, i.e. 0.1 pc. This corresponds to the typical size of the cores identified by Motte et al. The contribution of significant structures is continued up to 7–9′, i.e. 0.3–0.4 pc. This scale agrees with the size of the largest identified core. Above about 9′ the Δ-variance spectrum decays with $\alpha = -2$ indicating a lack of further correlated structure on larger scales. It is not clear whether the subtraction of large-scale emission unavoidable in the used observing mode has removed some large-scale correlation which is present in the cloud but cannot be detected from the map.

At small lags the spectrum indicates no separation between the scales where "cores" and "clumps" (condensations) were defined by Motte et al. The fit in Fig. 7 shows that on scales from 0.2′ to 2′, i.e. within a dynamic range of a factor ten, the spectrum is described by a single power-law smoothed by the observational beam. The Δ-variance spectrum suggests that the same processes drive the formation of the somewhat larger "cores" and the somewhat smaller condensations. The break in the spectrum at 0.4′, that seems to suggest a change in the scaling law of the observed structure, is only produced by the beam smearing and is quantitatively in agreement with a continuation of the power law observed on larger scales down to at least 0.2′. The underlying structure can be described by a perfect a power law in contradiction to the clump mass spectrum studied by Motte et al. who found a significant turn-down at a mass of about 0.5 $M_\odot$. This difference is even more intriguing because of the opposite situation in molecular line studies of the Polaris Flare where the clump mass spectrum shows a perfect power law (Heithausen et al. 1998) but the Δ-variance spectrum shows a steepening towards small scales (Bensch et al. 2001, see also Ossenkopf et al. 2000). From the theoretical modelling of the translation of a clump spectrum into a corresponding power spectral index of an fBm by Stutzki et al. (1998), we would expect a fixed relation between the measured clump mass spectrum and the corresponding Δ-variance spectrum in both cases. However, our examples violate this relation. The mass-size relation of the clumps may be affected by optical depth effects and a large part of the observationally identified clumps may result from the superposition of different structures along the line of sight, not well separated in velocity space (Ballesteros-Paredes & Mac Low 2002; Ossenkopf 2003). Further systematic studies are necessary to understand the actual physical processes interrelating the structure size spectra and the clump mass spectra.

We can compare the new results with the outcome of previous Δ-variance analyses, because all previous conclusions on the slopes of the Δ-variance spectra remain valid. The new Δ-variance method has improved our ability to precisely detect prominent scales, it has calibrated the absolute scales and it increased the statistical significance of the spectra by taking variable data reliability and edge effects into account, but none of these points should significantly affect the general scaling behaviour measured in our previous papers. The ρ Oph map shows a behaviour which is intermediate between that observed e.g. by Bensch et al. (2001) in molecular molecular lines, where we find a power-law Δ-variance spectrum on small scales and a dominance of large-scale structure, and the spectrum measured for the 1.3 mm continuum map of Serpens (Testi & Sargent 1998) analysed by Ossenkopf et al. (2001), where small cores dominate the spectrum resulting in a steep decay on large scales. In the ρ-Oph map we find both effects in one spectrum. The dense cores represent the dominating size scale but we can clearly resolve the scaling of significant structure on smaller scales.

Taking all facts from the scaling behaviour and the clump size detection together we conclude that an appropriate characterisation of the map in terms of a Δ-variance spectrum is only obtained when weighting the intensity maps by the inverse noise rms. Otherwise a variable noise in the spectra always tends to mimic small-scale structure which might be taken for real.

3.3. Velocity centroid maps

The situation is more difficult in the analysis of maps representing other quantities than intensities. Then the weighting function given by the inverse noise rms of the observation is not necessarily a good measure for the significance of the data. We study one such example here.

Investigating the velocity structure in the Polaris Flare molecular cloud, Ossenkopf & Mac Low (2002) applied the ordinary Δ-variance analysis to maps of centroid velocities in CO line data. The scaling behaviour of the velocity field measured in terms of the Δ-variance spectrum was compared to model simulations of interstellar turbulence. The data sets were given by three nested CO maps taken with different telescopes at different resolutions. The maps taken at high resolutions with the IRAM 30 m telescope (Falgarone et al. 1998) and the KOSMA 3 m telescope (Bensch et al. 2001) only covered regions with sufficiently bright emission so that a reliable determination of the line centroid velocities was possible at all points. The centroid Δ-variance spectra derived for these two maps showed a continuous power-law spectrum with a slight steepening towards the smallest lags.

In contrast, the map on the largest scale taken with the CfA 1.2 m telescope (Heithausen & Thaddeus 1990) contains many data points where no emission above the noise limit was detected. Moreover, it was difficult to obtain a reliable determination of the centroid velocities in regions where the line intensities only exceeded the noise rms by a factor of a few (see Ossenkopf & Mac Low 2002). The resulting Δ-variance spectrum did not show a continuation of the power-law behaviour from the two maps on smaller scales, but turned essentially flat. This is in contradiction to an eye inspection of the centroid map plotted in Fig. 8 showing a large-scale velocity gradient which should appear as well as large-scale structure in the Δ-variance spectrum. The corresponding map of line integrated intensities, plotted in Fig. 9, shows that the map contains large regions without emission. When the ordinary Δ-variance counts their centroid velocity with the same weight as that from points in the actual molecular cloud the "empty regions" statistically hide the variations in the regions with significant values. The virtual lack of large-scale velocity variations in the Δ-variance spectrum is thus due to the missing significance weighting.

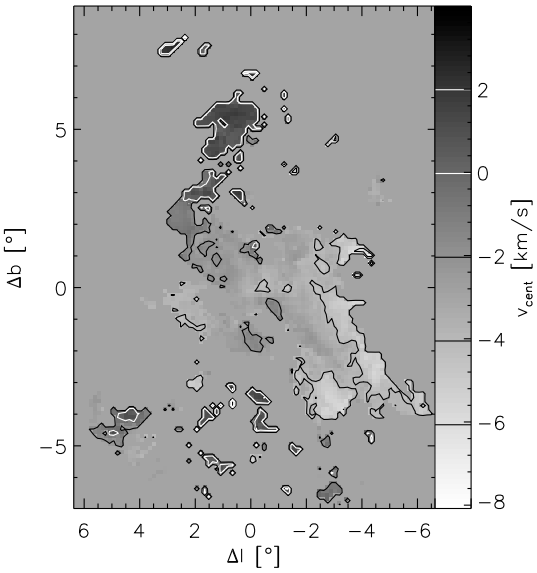

Fig. 8. Map of velocity centroids measured in the CO 1–0 map of the Polaris Flare taken with the CfA 1.4 m telescope (Heithausen & Thaddeus 1990). For all points with an integrated intensity below 0.65 K km s^{-1} a reasonable determination of the centroid velocity was impossible so that the average velocity of the cloud (–2.97 km s^{-1}) was assigned there. The axes are labelled relative to the zero position of l = 123.°628, b = 24.°93 in Galactic coordinates.

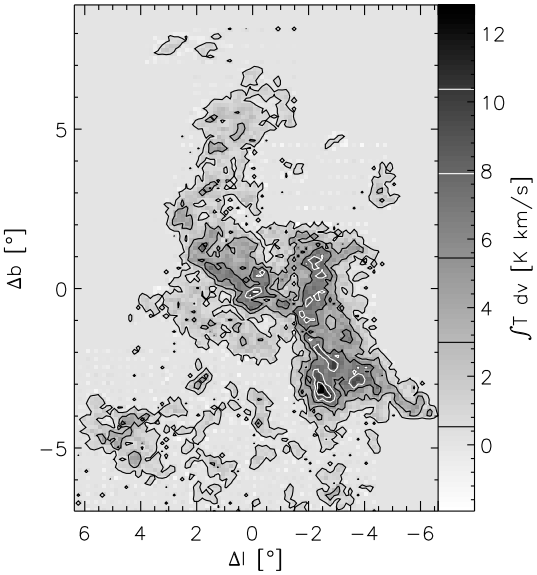

Fig. 9. CO 1–0 intensity map corresponding to the velocity centroid map in Fig. 8. The intensities provide a measure for the significance of the centroid velocities.

The knowledge on the reliability of the centroid velocities coming from the corresponding line intensities has to be taken into account using the improved Δ-variance analysis. Unfortunately, it is not obvious how the significance of the centroid velocities is related to the line intensities. We have tested weighting functions based on three assumptions: i) the significance of the centroid velocities is determined by the integrated line intensities at each point; ii) the zero value of the weighting

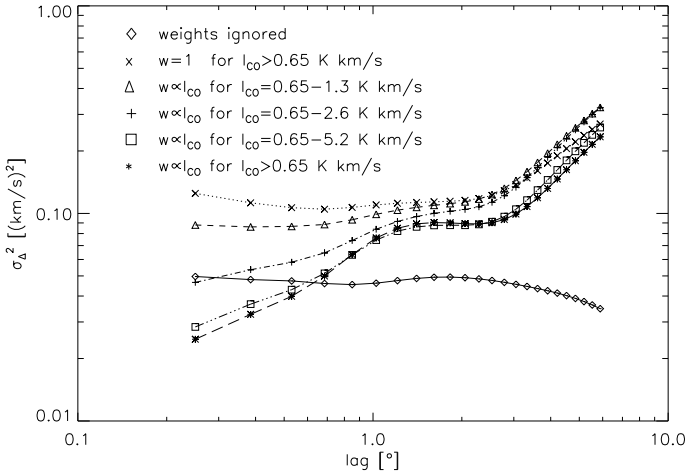

Fig. 10. Δ-variance spectra of the Polaris Flare velocity centroids computed with different weighting functions characterising the significance of the velocities at each point.

function corresponds to a minimum intensity of 0.65 K km s^{-1} which means that at least 10 velocity channels show an intensity above the noise rms; iii) Integrated intensities above some limit do not further increase the significance of the centroid velocities. The weighting function is unity at all points with higher intensities.

Figure 10 shows the resulting Δ-variance spectra of the centroid map when weighting functions with different upper intensity thresholds are applied. For an easy comparison to the previous results we also include the graph obtained without any weighting. The introduction of the weighting function results in a completely different Δ-variance spectrum at large lags. Whereas the previous computation showed a flat spectrum we find now a strong increase of the spectrum above 3°. Unfortunately, the results only give rough guidelines for the selection of the optimum weighting function. The best continuation of the Δ-variance spectra from the smaller scales provided by the KOSMA map is obtained when the upper intensity limit corresponds to four times the lower limit. The two curves only using a narrow dynamic intensity range for the weighting function are still heavily influenced by observational noise visible as increased Δ-variance values at small lags. On the other hand it is not clear whether the complete suppression of the noise effect in the two curves with the highest upper limits is realistic, so that we conclude that in this example the significance of the centroid velocities does not further increase for integrated intensities above 2.6 K km s^{-1}. Nevertheless, a final answer to this question still has to come from a theoretical model for the quantitative impact of the observational noise on the noise in centroid velocities.

In spite of the uncertainty of the noise contribution at small lags, we can draw new essential conclusions on the velocity structure of the Polaris Flare from the Δ-variance spectrum. The power-law scaling behaviour of the velocity structure detected previously only for smaller sizes is now continued up to scales of 1.3°, i.e. 3–4 pc. A single power law with an exponent $\alpha \approx 0.9$ can be used to cover the length scale range of about a factor 100. The Δ-variance spectrum also shows a plateau around 2°, i.e. 5 pc, indicating the relative deficiency of motions on that scale. Above 3° the Δ-variance spectrum rises again tracing the global velocity gradient visible in Fig. 8. This behaviour indicates that the large-scale gradient is not converted directly by shear motions into the turbulent cascade but that the turbulent cascade starts at somewhat smaller scales. This points towards a shock producing the large-scale gradient which is only converted into turbulent energy on the scale of previously existing density fluctuations in the cloud and excludes Galactic rotation as the main driving force.

4. Conclusions

In Paper I we have proposed two essential improvements of the Δ-variance analysis. Here, we have tested their actual impact when applied to data sets characterising interstellar turbulence.

The first improvement was the introduction of a weighting function for each pixel in the map. This allows us to study data sets with a variable data reliability across the map and to simultaneously solve boundary problems even for maps with irregular boundaries. Maps with a variable data reliability are eventually obtained in most observations, either due to a local or a temporal variability of the detector sensitivity or the atmosphere or due to different integration times spent for different points of a map. By applying the improved Δ-variance analysis to observed data we find that only the use of a significance function to weight the different data points allows us to distinguish the influence of variable noise from actual small-scale structure in the maps. In the analysis of intensity maps the weighting function is best provided by the inverse rms in the data points. The situation is more complex for derived quantities, like centroid velocities, without a simple analytic relation between the uncertainty of the quantity and the observational noise. Here, in general two thresholds can be defined – a lower threshold below which all data have to be ignored and an upper threshold above which the significance of the data is not further improved by decreasing the noise. For the centroid velocities this means that the integrated line intensities between the two boundaries may serve as weighting function.

The second improvement of the Δ-variance analysis is its optimisation with respect to the shape of the wavelet used to filter the observed maps. The application of different filters in the analysis of hydrodynamic simulations confirmed the result from Paper I, that a Mexican-hat filter with a diameter ratio $v = 1.5$ is well suited to resolve prominent structure scales and to measure the slope of the turbulent cascade, however, it turned out that the impact of the detailed shape of the Δ-variance filter is less significant for realistic data than for the artificial test data used in Paper I. The turbulent structure is well resolved for a wide set of filters as long as one consistent filter shape is used throughout the full analysis of a data set. Comparing the density and velocity structure of the simulations shows a small but significant shift between the scale of the most prominent velocity structures, created by the energy injection, and the most prominent density structures produced by the velocity field.

Applying the new method to the example of the dust emission map of ρ Oph by Motte et al. (1998) shows that the spatial scaling behaviour there can be described perfectly by a power law interconnecting the range of small clumps and more massive cores. The method can reproduce the size of the dominant cores and we find no indication for large-scale correlation between the clumps and cores in the data. The Δ-variance spectrum shows no break in the scaling behaviour between cores and condensations in contrast to the mass spectrum derived by Motte et al. (1998). The reason for the different behaviour of the two measures has to be topic of a future investigation.

In the example of the analysis of the velocity structure in the Polaris Flare we show that the power-law scaling behaviour established by Ossenkopf & Mac Low (2002) for the small scales is continued to large scales. However, a plateau in the Δ-variance

spectrum around 5 pc indicates that the existing large-scale velocity gradient is not converted directly into a turbulent cascade. A possible explanation for this behaviour is the existence of a shock producing the large-scale gradient which is only converted into turbulent energy on the scale of the individual density fluctuations in the cloud. This scenario would be consistent with the affiliation of the molecular cloud to a large HI supershell by Meyerdierks et al. (1991).

Combining the results from the turbulence simulation with the analysis of the Polaris Flare velocity structure indicates that a large-scale velocity field does not automatically produce density structures on those scales, but that a full turbulence cascade covering density and velocity fluctuations evolves predominantly at seeds of primordially existing density fluctuations, which may have been produced by previous velocity fields on larger scales. When interpreting turbulent structures in interstellar clouds it has to be taken into account that close to the scale of the energy injection a statistical analysis of the turbulent cascade is always affected by low number statistics as few density "seeds" may dominate the shape of the scaling relations there. A reliable statistics is only given on smaller scales.

Acknowledgements. We thank R. Klessen for providing us with the numerical data of the SPH simulations used in Sect. 3.1. We thank Ph. André for the data of the ρ Oph continuum observations used in Sect. 3.2. We thank F. Bensch for useful discussions and J. Ballesteros-Paredes for carefully refereeing this paper suggesting significant improvements. This work has been supported by the Deutsche Forschungsgemeinschaft through grant 494B. It has made use of NASA's Astrophysics Data System Abstract Service.

References

Ballesteros-Paredes, J., & Mac Low, M.-M. 2002, ApJ, 570, 734B
Bensch, F., Stutzki, J., & Ossenkopf, V. 2001, A&A, 366, 636
Décamp, N., & Le Bourlot, J. 2002, A&A, 389, 1055
Elmegreen, B. G., & Scalo, J. 2004, ARA&A, 42, 211
Falgarone, E., & Panis, J.-F., Heithausen, A., et al. 1998, A&A, 331, 669
Falgarone, E., Hily-Blant, P., & Levrier, F. 2004, Ap&SS, 292, 89
Franco, J., & Carramiñana, A. 1999, Interstellar Turbulence (Cambridge Univ. Press)
Heithausen, A., & Thaddeus, P. 1990, ApJL, 353, L49
Heithausen, A., Bensch, F., Stutzki, J., Falgarone, E., & Panis, J. F. 1998, A&A, 331, L65
Klessen, R. S., Heitsch, F., & Mac Low, M.-M. 2000, ApJ, 535, 887
Kramer, C., Stutzki, J., Röhrig, R., & Corneliussen, U. 1998, A&A, 329, 249
Mac Low, M.-M., & Ossenkopf, V. 2000, A&A, 353, 339
Mac Low, M.-M., & Klessen, R. S. 2004, RvMP, 76, 125
Meyerdiercks, H., Heithausen, A., & Reif, K. 1991, A&A, 245, 247
Motte, F., André, P., & Neri, R. 1998, A&A, 336, 150
Ossenkopf, V. 2003, in Galactic Star Formation Across the Stellar Mass Spectrum, ed. J. M. De Buizer, & N. S. van der Bliek, ASP Conf., 287, 19
Ossenkopf, V., & Mac Low, M.-M. 2002, A&A, 390, 307
Ossenkopf, V., Bensch, F., & Stutzki, J. 2000, in The Chaotic Universe (World Sci.), ed. V. G. Gurzadyan, & R. Ruffini, 394
Ossenkopf, V., Klessen, R., & Heitsch, F. 2001, A&A, 379, 1005
Ossenkopf, V., Krips, M., & Stutzki, J. 2008, A&A, 485, 917 (Paper I)
Stutzki, J., & Güsten, R. 1990, ApJ, 356, 513
Stutzki, J., Bensch, F., Heithausen, A., Ossenkopf, V., & Zielinsky, M. 1998, A&A, 336, 697
Testi, L., & Sargent, A. 1998, ApJ, 508, L91
Vázquez-Semadeni, E., Ballesteros-Paredes, J., & Rodrìguez, L. F. 1997, ApJ, 474, 292